Thermoelastic Properties of Ringwoodite $(Fe_x,Mg_{1-x})_2SiO_4$: Its Relationship to the 520 km Seismic Discontinuity.

Maribel Núñez Valdez[a,*], Zhongqing Wu[b,c], Yonggang G. Yu[c], Justin Revenaugh[d], Renata M. Wentzcovitch[c,e]

[a] *School of Physics and Astronomy, University of Minnesota, Minneapolis, MN 55414, USA*
[b] *School of Earth and Space Sciences, University of Science and Technology of China, Hefei, Anhui 230026, China*
[c] *Department of Chemical Engineering and Materials Science, University of Minnesota, Minneapolis, MN 55414, USA*
[d] *Department of Earth Sciences, University of Minnesota, Minneapolis, MN 55414, USA*
[e] *Minnesota Supercomputing Institute, University of Minnesota, Minneapolis, MN 55414, USA*

Abstract

We combine density functional theory (DFT) within the local density approximation (LDA), the quasiharmonic approximation (QHA), and a model vibrational density of states (VDoS) to calculate elastic moduli and sound velocities of $\gamma-(Fe_x,Mg_{1-x})_2SiO_4$ (ringwoodite), the most abundant mineral of the lower Earth's transition zone (TZ). Comparison with experimental values at room-temperature and high pressure or ambient-pressure and high temperature shows good agreement with our first-principles findings. Then, we investigate the contrasts associated with the $\beta \rightarrow \gamma(Fe_x,Mg_{1-x})_2SiO_4$ transformation at pressures and temperatures relevant to the TZ. This information offers clearly defined reference values to advance the understanding

*Corresponding author. Tel.: +1 612 624 2872; fax: +1 612 626 7246
Email address: valdez@physics.umn.edu (Maribel Núñez Valdez)

of the nature of the 520 km seismic discontinuity.

Keywords: first principles, ringwoodite, elasticity, transition zone, 520 km discontinuity

1. Introduction

Wadsleyite (β-phase) and ringwoodite (γ-phase) are the high-pressure polymorphs of olivine (α-phase), $(Fe_x,Mg_{1-x})_2SiO_4$. These minerals are the main constituents of the Earth's upper mantle (UM) (Rinwood, 1975; Putnis, 1992) and transition zone (TZ) (Irifune and Ringwood, 1987). Under pressure, the transformation from olivine to wadsleyite happens at ∼13.5 GPa and from wadsleyite to ringwoodite at ∼18 GPa near 1600 K (Katsura and Ito, 1989; Akaogi et al., 1989). These transformations are associated with two major discontinuities in seismic velocities in the Earth's interior at about 410 km and 520 km depth, respectively (Revenaugh and Jordan, 1991). While the first discontinuity is a well characterized and sharp feature in seismic data, the second varies considerably with location.

Experimental and computational approaches have been used to study properties of these minerals at *in situ* conditions and their relationship with seismic discontinuities. Mg-end member and Fe-bearing α-phases have been widely investigated at simultaneous high pressure and temperature. Computational results and experimental data on elastic properties and sound velocities seem to be consistent with seismic measurements (see e.g. Núñez Valdez et al., 2010; Stackhouse et al., 2010; Li and Liebermann, 2007, and references there in). On the other hand, even though great efforts have been made to obtain measurements of elastic properties and wave velocities of Fe-free and

Fe-bearing wadsleyite and ringwoodite under high temperature and pressure using either ultrasonic or Brillouin scattering techniques (Li et al., 1996; Zha et al., 1997; Isaak et al., 2007; Sinogeikin et al., 1998; Li and Liebermann, 2000; Liu et al., 2009; Mayama et al., 2004; Isaak et al., 2010; Li, 2003; Higo et al., 2006; Weidner et al., 1984; Sinogeikin et al., 2003; Jackson et al., 2000; Mayama et al., 2005), results are still limited. Therefore large extrapolations from room conditions to conditions of the TZ are often used.

First principles calculations employing the quasiharmonic approximation (QHA), valid up to about two thirds of the melting temperature, or molecular dynamics (MD) methods, valid near and above melting temperatures, complement each other and are used to obtain elastic moduli under high-pressure-temperature conditions. Calculations of elastic constants using the QHA, though computationally less demanding than MD, still required calculations of vibrational density of states (VDoS) for each strained atomic configuration at several pressures, that is, about 1000 parallel jobs (Da Silveira et al., 2008, 2011).

In this paper we use the analytical and computational approach by Wu and Wentzcovitch (2011) and tested on periclase-MgO, $\alpha-Mg_2SiO_4$, and more recently on $\beta-(Fe_x,Mg_{1-x})_2SiO_4$ (Núñez Valdez et al., 2012), to calculate bulk (K) and shear (G) moduli and sound velocities of the $\gamma-(Fe_x,Mg_{1-x})_2SiO_4$ phase. This method uses only static elastic constants and phonon density of states for unstrained configurations, therefore reducing the amount of computational time and resources by one to two orders of magnitude. We then address contrasts across the $\beta \rightarrow \gamma(Fe_x,Mg_{1-x})_2SiO_4$ transition near conditions of the 520 km seismic discontinuity.

2. Methodology

2.1. Computational Details

Calculations based on Density Functional Theory (DFT) (Hohenberg and Kohn, 1964; Kohn and Sham, 1965) were performed using the local density approximation (LDA) (Ceperley and Alder, 1980). Ultrasoft pseudopotentials generated by the Vanderbilt method (Vanderbilt, 1990) were used to describe Fe, Si, and O. A norm-conserving pseudopotential generated by the von Car method was used for Mg. Further details about these pseudopotentials are given in (Núñez Valdez et al., 2011). Equilibrium structures of ringwoodite (28 atoms/cell) at arbitrary pressures were found using the variable cell-shape damped molecular dynamics approach (Wentzcovitch, 1991; Wentzcovitch et al., 1993) as implemented in the quantum-ESPRESSO (QE) code (Giannozzi et al., 2009). The plane-wave kinetic energy cutoff used was 40 Ry and for the charge density 160 Ry. The **k**-point sampling of the charge density was determined on a $2 \times 2 \times 2$ Monkhorst-Pack grid of the Brillouin Zone (BZ) shifted by $\left(\frac{1}{2}\frac{1}{2}\frac{1}{2}\right)$ from the origin. These parameters correspond to having interatomic forces smaller than 10^{-4} Ry/a.u. and pressure convergence within 0.5 GPa. Dynamical matrices were obtained using density functional perturbation theory (DFPT) (Baroni et al., 2001) via QE. At each pressure, a dynamical matrix was calculated on a $2 \times 2 \times 2$ **q**-point mesh for one atomic configuration only. In principle about 10 other configurations should be used as well, but here we are more interested in frequencies with strain and the current approximation seems to be sufficiently accurate. Force constants were extracted and interpolated to a $12 \times 12 \times 12$ regular **q**-point mesh to produce VDoS.

2.2. High-Temperature-Pressure Elastic Theory

Exploiting the information about the strain and volume dependence of phonon frequencies, we determine the thermal contribution to the Helmholtz free energy F within the QHA (Wallace, 1972), that is,

$$F\left(e,V,T\right)=U_{st}(e,V)+\frac{1}{2}\sum_{\mathbf{q},m}\hbar\omega_{\mathbf{q},m}(e,V)+$$
$$+k_BT\sum_{\mathbf{q},m}\ln\left\{1-exp\left[-\frac{\hbar\omega_{\mathbf{q},m}(e,V)}{k_BT}\right]\right\}, \tag{1}$$

where $\mathbf{q}$ is the phonon wave vector, m is the normal mode index, T is temperature, U_{st} is the static internal energy at equilibrium volume V under isotropic pressure P and infinitesimal strain e, $\hbar$ and k_B are Planck and Boltzmann constants, respectively. Isothermal elastic constants are given by

$$C^T_{ijkl}=\left[\frac{\partial^2G(P,T)}{\partial e_{ij}e_{kl}}\right]_P, \tag{2}$$

with $G=F+PV$, the Gibbs energy, and $i,j,k,l=1,\ldots,3$. To convert to adiabatic elastic constants, one uses the relationship:

$$C^S_{ijkl}=C^T_{ijkl}+\frac{T}{VC_V}\frac{\partial S}{\partial e_{ij}}\frac{\partial S}{\partial e_{kl}}\delta_{ij}\delta_{kl}, \tag{3}$$

where C_V is heat capacity at constant volume, and S is entropy. For orthorhombic crystals, the non-shear elastic constants of Eq. (2) are:

$$\begin{aligned} C^T_{iijj} &= \left[\frac{\partial^2F(\mathbf{e},V,T)}{\partial e_{ii}e_{jj}}\right]_P+(1-\delta_{ij})P(V,T), \\ &= C^{st}_{iijj}(V)+C^{ph}_{iijj}(V,T), \end{aligned} \tag{4}$$

while the shear elastic constants are:

$$C^T_{ijij}=C^{st}_{ijij}(V)+C^{ph}_{ijij}(V,T). \tag{5}$$

Elastic constants C^{ph}_{iijj} and C^{ph}_{ijij} can be expressed as functions of the volume Grüneisen parameters, $\gamma_{\mathbf{q},m} = -\partial(\ln \omega_{\mathbf{q},m})/\partial(\ln V)$:

$$\frac{d\omega_{\mathbf{q},m}}{\omega_{\mathbf{q},m}} = -\gamma_{\mathbf{q},m}\frac{dV}{V}, \tag{6}$$

or the generalization to strain Grüneisen parameters:

$$\frac{\partial\omega_{\mathbf{q},m}}{\omega_{\mathbf{q},m}} = -\gamma^{ij}_{\mathbf{q},m}e_{ij}. \tag{7}$$

We have used the Wu-Wentzcovitch method (Wu and Wentzcovitch, 2011) to compute the thermal contribution to the elastic constants, $C^{ph}_{ijij}(V,T)$. This method allows the computation of thermal elastic constants without performing phonon calculations for strained configurations with the approximation that strain and mode Grüneisen parameters have isotropic distribution, which is equivalent to assuming that thermal pressure is isotropic. This is a good approximation (Carrier et al., 2007) implicit in the QHA calculation of thermal pressures.

After obtaining VDoS at several volumes by first principles, average strain Grüneisen parameters were computed at such volumes and interpolated in a fine volume-temperature grid, that was then inverted to a pressure-temperature grid of 0.1 GPa and 10 K spacings. Static elastic constants previously computed (Núñez Valdez et al., 2011) were also used.

Voigt and Reuss bounds of bulk and shear moduli of orthorhombic crystals at high temperature were calculated using adiabatic elastic constants as

(Watt et al., 1976; Watt, 1979):

$$K_V = \frac{1}{9}\left[C_{11} + C_{22} + C_{33} + 2\left(C_{12} + C_{13} + C_{23}\right)\right], \tag{8}$$

$$\begin{aligned} G_V = & \frac{1}{15}\left[C_{11} + C_{22} + C_{33} + 3\left(C_{44} + C_{55} + C_{66}\right)\right. \\ & \left. - \left(C_{12} + C_{13} + C_{23}\right)\right], \end{aligned} \tag{9}$$

$$\begin{aligned} K_R = & D\left[C_{11}\left(C_{22} + C_{33} - 2C_{23}\right) + C_{22}\left(C_{33} - 2C_{13}\right)\right. \\ & -2C_{33}C_{12} + C_{12}\left(2C_{23} - C_{12}\right) \\ & \left. + C_{13}\left(2C_{12} - C_{13}\right) + C_{23}\left(2C_{13} - C_{23}\right)\right]^{-1}, \end{aligned} \tag{10}$$

$$\begin{aligned} G_R = & 15\left\{4\left[C_{11}\left(C_{22} + C_{33} + C_{23}\right) + C_{22}\left(C_{33} + C_{13}\right)\right.\right. \\ & + C_{33}C_{12} - C_{12}\left(C_{12} + C_{23}\right) - C_{13}\left(C_{13} + C_{12}\right) \\ & \left.\left. - C_{23}\left(C_{23} + C_{13}\right)\right]/D\right. \\ & \left. + 3\left(1/C_{44} + 1/C_{55} + 1/C_{66}\right)\right\}^{-1}, \end{aligned} \tag{11}$$

$$\begin{aligned} D = & C_{13}\left(C_{12}C_{23} - C_{13}C_{22}\right) + C_{23}\left(C_{12}C_{13} - C_{23}C_{11}\right) \\ & + C_{33}\left(C_{11}C_{22} - C_{12}^2\right). \end{aligned} \tag{12}$$

With Voight-Reuss-Hill averages of elastic moduli, i.e.,

$$K = \frac{K_V + K_R}{2} \text{ and } G = \frac{G_V + G_R}{2}, \tag{13}$$

isotropic sound velocities are given by:

$$V_P = \sqrt{\frac{K + \frac{4}{3}G}{\rho}}, \quad V_S = \sqrt{\frac{G}{\rho}}, \quad V_\Phi = \sqrt{\frac{K}{\rho}}, \tag{14}$$

where ρ is density, and V_P, V_S, and V_Φ are compressional, shear and bulk velocities, respectively.

3. Results

We present first-principles results of aggregate properties of Fe-bearing ringwoodite at pressures and temperatures relevant to the TZ. All the ap-

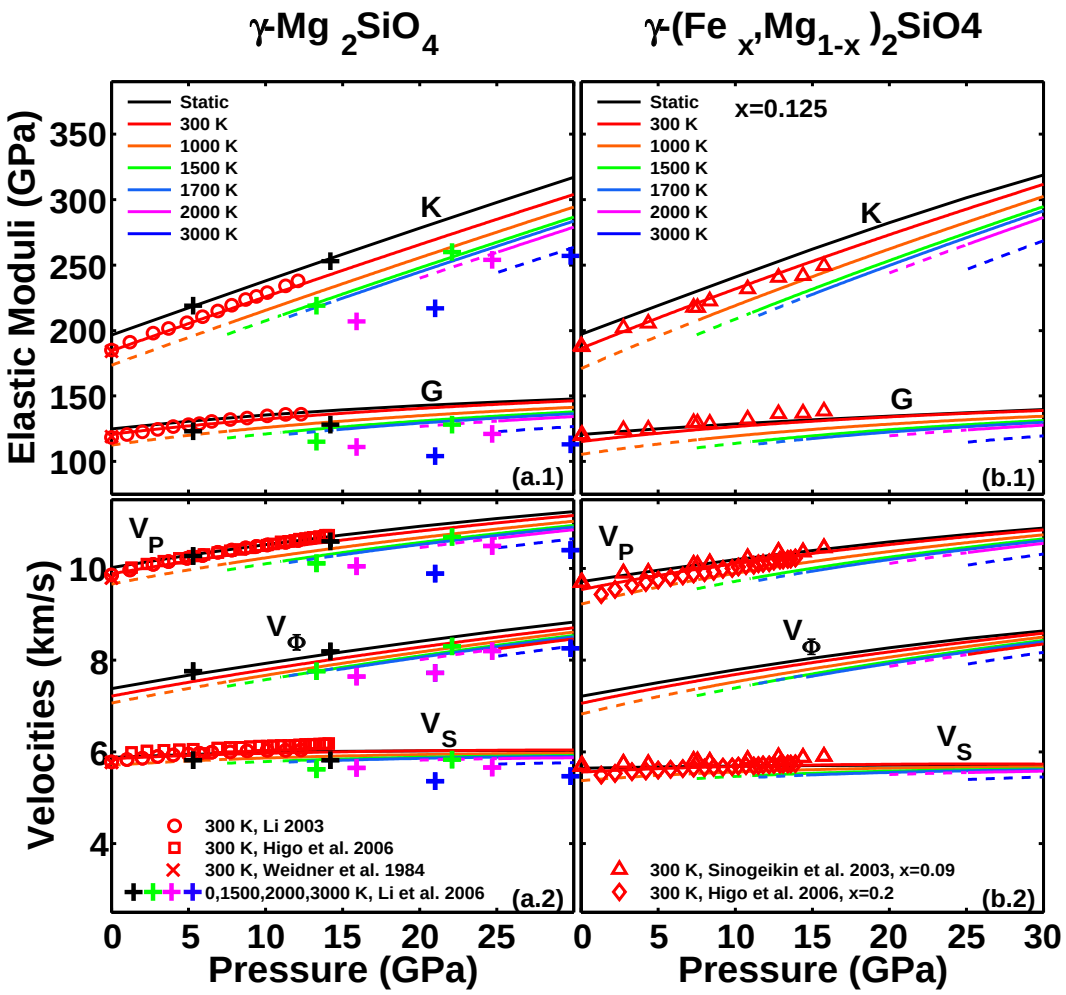

Figure 1: (Color online) Pressure and temperature dependence of bulk modulus (K), shear modulus (G), compressional velocity (V_P), shear velocity (V_S) and bulk velocity (V_Φ) for Fe-free ringwoodite (a,c) and Fe-bearing ringwoodite (b,d). First principles calculations within LDA (solid lines) are compared to available experimental data (symbols). Note, however, that low-pressure-high temperature calculated trends (dash lines) are outside the validity of the QHA.

proximations described in the previous section provided an excellent description of bulk and shear moduli, and sound velocities within the valid regime of the QHA established for the Fe-free quantities (Yu et al., 2008) for $\gamma-(Fe_x,Mg_{1-x})_2SiO_4$ with $x = 0$ and $x = 0.125$ (see Figs. 1 and 2).

In the case of the Mg-end member ringwoodite, K increases more rapidly than G, as a function of pressure, and decreases faster than G with increasing temperature. At 300 K the agreement between experimental data (Li, 2003; Higo et al., 2006; Weidner et al., 1984) and our DFT-results is truly excellent for elastic moduli (Fig. 1a), and sound velocities (Fig. 1c). Results from a molecular dynamics study by Li et al. (2006) also compare well with our results for K, V_P, and V_Φ within the QHA limits. Our predicted G and V_S are larger and smaller, respectively, than molecular dynamics values Li et al. (2006). This difference is primarily caused by the use of the GGA approximation in the MD simulation. Nevertheless the general agreement is good and it is the only other source to compare aggregate properties of $\gamma-Mg_2SiO_4$ at high pressures and temperatures. Results of Fe-bearing ringwoodite as function of pressure are shown in Figs. 1b and 1d. Experimental data by Sinogeikin et al. (2003) at room temperature and $x = 0.09$ are in excellent agreement with our 300 K curve, though after 10 GPa our K tends to be larger, while G tends to be smaller (Fig. 1b). Fe-bearing compressional, shear and bulk velocities are smaller than their Fe-free counterparts (Fig. 1d). Predictions for $x = 0.125$ fall in between two experimental reports with iron concentrations of $x = 0.09$ (Sinogeikin et al., 2003) and $x = 0.2$ (Higo et al., 2006). From Fig. 1d one can see that V_P is the most affected by iron concentration and temperature, while V_S seems to be the least affected

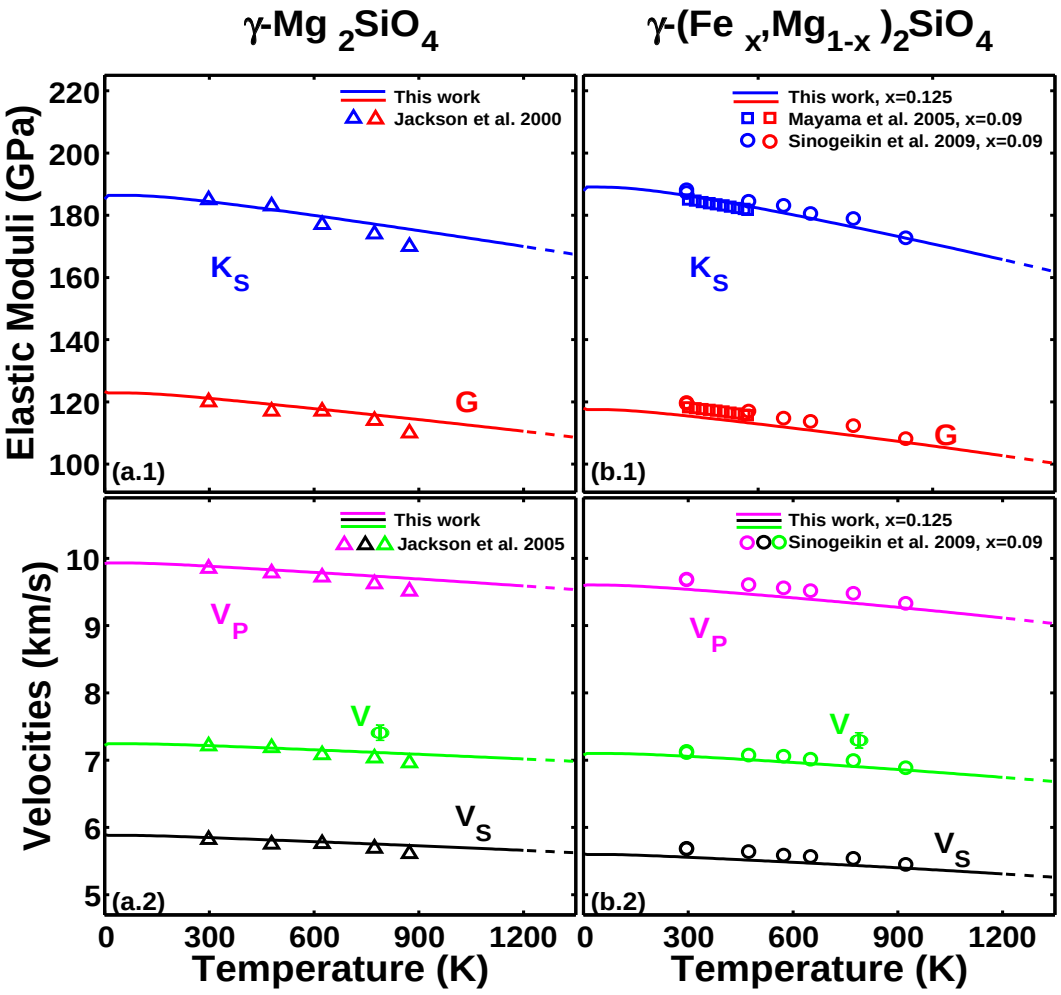

Figure 2: (Color online) Temperature dependence of bulk modulus (K), shear modulus (G), compressional velocity (V_P), shear velocity (V_S) and bulk velocity (V_Φ) for Mg-end member ringwoodite (a,c) and Fe-bearing ringwoodite (b,d). First principles calculations within LDA (solid lines) are compared to available experimental data (symbols) at P=0 GPa.

by these two factors.

The temperature dependence of elastic moduli and sound velocities of Fe-free and Fe-bearing ringwoodite at ambient pressure are shown in Fig. 2. For $x = 0$, the agreement between experimental results (Jackson et al., 2000) and our findings is outstanding (Figs. 2a and 2c). Similarly, our predicted aggregate properties for $x = 0.125$ are in excellent correspondence with experiments having $x = 0.09$ (Mayama et al., 2005; Sinogeikin et al., 2003) (Figs. 2b and 2d). Predicted Fe-bearing K is larger than Fe-free K at 300 K (Table 1), and dK/dT is more negative for $x = 0.125$ than for $x = 0$. On the other hand, G decreases with iron, but likewise K, dG/dT is more negative for $x = 0.125$ than for $x = 0$. Predicted compressional, shear, and bulk velocities as function of temperature are smaller than those reported by Sinogeikin et al. (2003), which can be understo0d given the difference in iron content (Fig. 2d). The x dependence of elastic moduli and velocities for $\alpha-$, $\beta-$, and $\gamma-(\mathrm{Fe}_x,\mathrm{Mg}_{1-x})_2\mathrm{SiO}_4$ at high temperatures and pressures is shown in Fig. 3. We find dK/dx to be positive for all three phases, while dG/dx, dV_P/dx, dV_S/dx, and dV_Φ/dx are negative. For small x, a linear trend given by our results of elastic moduli and velocities compares well to experimental data of olivine and ringwoodite. On the other hand, experimental values of wadsleyite are more scattered and deviate the most from the proposed linear behavior. Detailed dependence on pressure and temperature of dK/dx, dG/dx, dV_P/dx, dV_S/dx, and dV_Φ/dx are shown in Figs. 4 and 5. dK/dx and dG/dx for all three phases exhibit qualitatively similar behavior in the pressure range considered. At low pressure they are quite sensitive to temperatures, but they seem to converge at high pressure

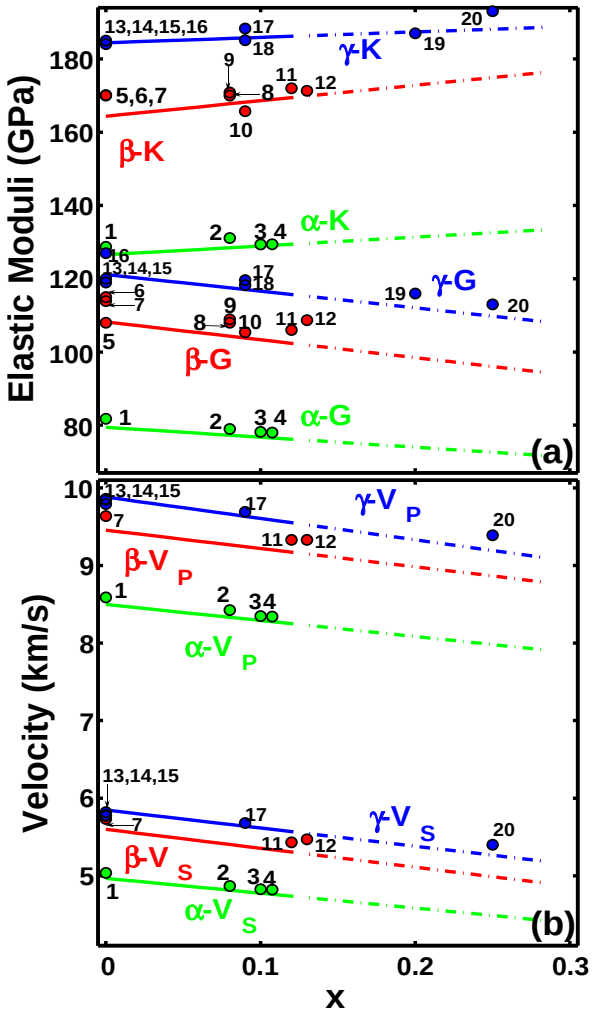

Figure 3: (Color online) Dependence on low iron content at $P = 0$ GPa and $T = 300$ K of a) elastic moduli, K and G, and b) velocities, V_P and V_S, (lines) compared to experimental data (circles): 1-Isaak et al. (1989); 2,3-Isaak (1992); 4-Abramson et al. (1997); 5-Li et al. (1996); 6-Zha et al. (1997); 7-Isaak et al. (2007); 8-Sinogeikin et al. (1998); 9-Isaak et al. (2010); 10-Mayama et al. (2004); 11-Li and Liebermann (2000); 12-Liu et al. (2009); 13-Weidner et al. (1984); 14-Jackson et al. (2000); 15-Li (2003); 16,19-Higo et al. (2006); 17-Sinogeikin et al. (2003); 18-Mayama et al. (2005); 20-Sinogeikin et al. (1997).

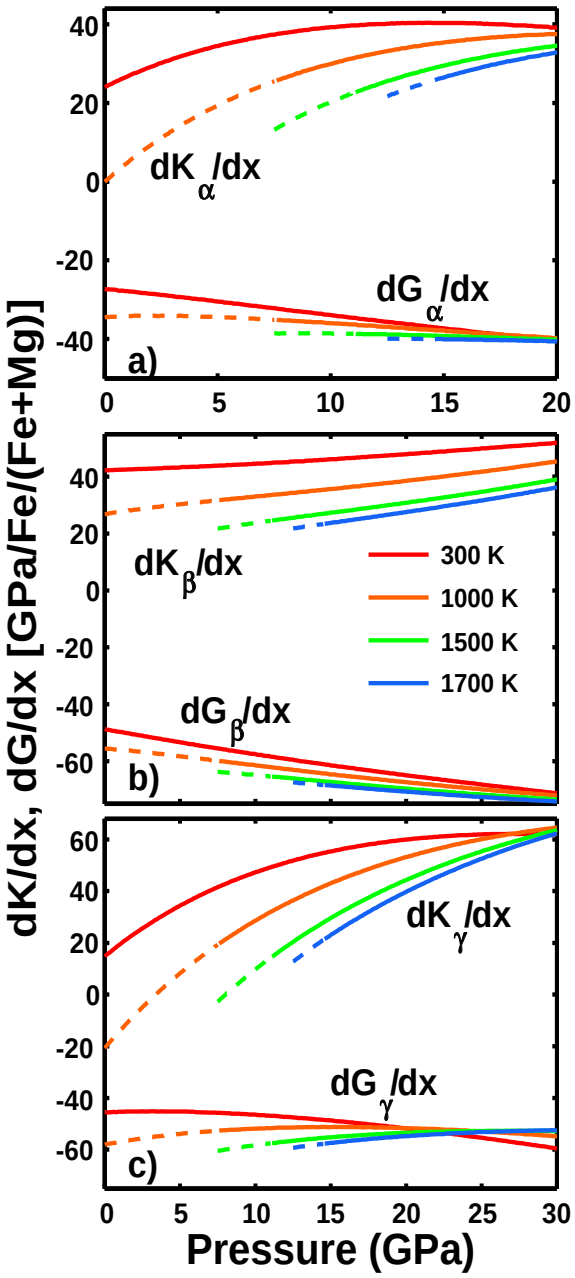

Figure 4: (Color online) Pressure dependence of dK/dx and dG/dx for a) olivine, b) wadsleyite, and c) ringwoodite.

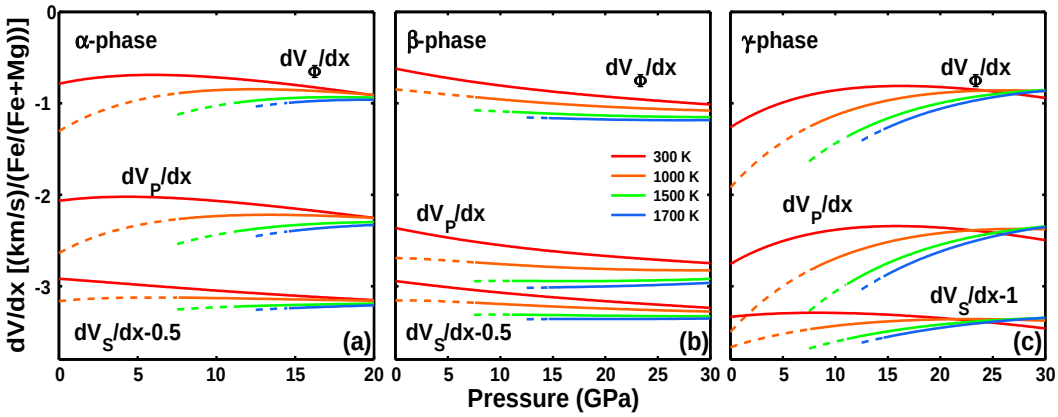

Figure 5: (Color online) Pressure dependence of dV/dx for a) olivine, b) wadsleyite, and c) ringwoodite.

(Figs. 4a and 4c). dV_P/dx, dV_S/dx, and dV_Φ/dx for all three phases are also more sensitive to temperature at lower pressures.

4. Geophysical implications: The 520 km Discontinuity

The seismic discontinuity near 520 km depth is often attributed to the phase change of wadsleyite to ringwoodite (Katsura and Ito, 1989; Shearer, 1990; Revenaugh and Jordan, 1991). It is more likely to be unobserved than either of its near neighbors at 410-km and 660-km depth. It is, on average, a smaller amplitude feature (e.g. Revenaugh and Jordan, 1991) such that less frequent observation is to be expected. In some studies the 520 km discontinuity appears as a split arrival or doublet (e.g. Deuss and Woodhouse, 2001; Chambers et al., 2005; Bagley et al., 2009). When split, the two discontinuities are observed at depths of approximately 500 and 560 km (Deuss and Woodhouse, 2001). Notably the sum of the two seismic features is larger than typical

non-split observations. Whether this is the result of an upward bias in identifying split arrivals or the result of greater net velocity contrast it is not clear. Therefore accurate data on elasticity of wadsleyite and ringwoodite are critical for investigating the role of the transformation $\beta \rightarrow \gamma$ on the 520 km seismic discontinuity. We use our results on aggregate properties of $\beta-$ (Núñez Valdez et al., 2012) and $\gamma-(Fe_x,Mg_{1-x})_2SiO_4$ at temperatures and pressures encompassing the TZ to estimate the magnitude of the discontinuity across the phase transition. Although this is a divariant phase transition and calculation of the two-phase loop is beyond the scope of this work, we can clearly calculate velocity increases throughout the entire transition. As we saw in the previous section, experimental studies dealing with simultaneous high pressures and temperatures offer limited data, and analyses usually extrapolate results at ambient conditions either in temperature or pressure to conditions near 520 km depth ($\sim$18 GPa and $\sim$1600 K). The lack of other source of knowledge makes it difficult to outline conclusions and/or explain the nature of the 520 km seismic discontinuity. With this paper we hope to advance the understanding of this discontinuity.

To quantify the magnitude of the discontinuity across the β to γ transition at finite temperatures we use the contrast Δ of a particular property M defined as:

$$\Delta M = \frac{(M_{x,\gamma} - M_{x,\beta})}{\frac{(M_{x,\beta}+M_{x,\gamma})}{2}} \times 100, \tag{15}$$

where M could be density, elastic modulus, or velocity. Table 2 and Fig. 6 show our calculated contrasts at finite temperatures for the $\beta \rightarrow \gamma$ transition in Fe-free and Fe-bearing phases. We first notice that $\Delta\rho$ is almost independent of temperature and pressure with iron having an insignificant

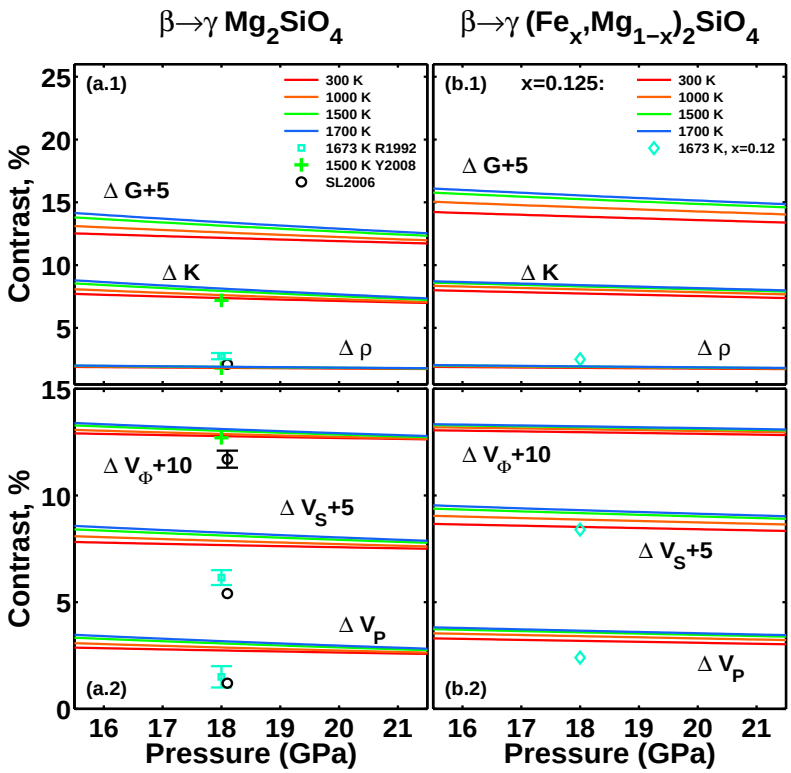

Figure 6: (Color online) Density, elastic, and velocity contrasts (lines) compared to laboratory and seismic data across the Fe-free (a,c) and Fe-bearing (b,d) $\beta \rightarrow \gamma$ transition. R1992: Rigden et al. (1992); Y2008: Yu et al. (2008); SL2006: Lawrence and Shearer (2006); $x = 0.12$: Sinogeikin et al. (2003).

effect (Figs. 6a and 6b), as suggested by Yu et al. (2008). Extrapolated experimental results and seismic data also suggested that iron should have a small effect on this quantity (Rigden et al., 1991; Lawrence and Shearer, 2006; Sinogeikin et al., 2003). For $x = 0$ we obtain a very good agreement with a previous estimation by Yu et al. (2008). For $x = 0.125$ our result is slightly smaller than that by Sinogeikin et al. (2003) for $x = 0.09$. Contrasts of elastic moduli (Figs. 6a and 6b) indicate that ΔG is more sensitive to temperature than ΔK. This dependence is greater in $x = 0.125$ than in $x = 0$. In the 16–21GPa range, both ΔG and ΔK slightly decrease with pressure, irrespective of x. Figs. 6c and 6d show that velocity contrasts, ΔV_P, ΔV_S, and ΔV_Φ, exhibit weak pressure dependence, decreasing only slightly with pressure. Temperature affects ΔV_S more than ΔV_P or ΔV_Φ. For $x = 0$, a comparison of our results to extrapolations of experimental data by Rigden et al. (1991) to 18 GPa and 1673 K and seismic data by Lawrence and Shearer (2006) shows predicted contrasts to be larger. ΔV_Φ is in better agreement with a previous prediction at 1700 K (Yu et al., 2008) and with a contrast from seismic studies (Lawrence and Shearer, 2006). Velocity contrasts increase with increasing x, however ΔV_S is the most enhanced by x, followed by ΔV_P, and ΔV_Φ. Extrapolations of ΔV_P and ΔV_S to 18 GPa and 1673 K with $x = 0.12$ reported by Sinogeikin et al. (2003) are smaller than our predicted contrasts, though ΔV_S is closer to our prediction.

In an attempt to explain the presence of two mid-transition zone discontinuities, Saikia et al. (2008) investigated the solubility of $CaSiO_3$ perovskite in majorite garnet at high-pressure (15–24 GPa) and high-temperature (1400° C–1600° C). They concluded that in fertile peridotite (i.e., peridotite en-

$\beta-(Mg_{1-x},Fe_x)_2SiO_4$				
V (Å^3)	K (GPa)	G (GPa)	x	Reference
541.3	164.4	107.7	0	Núñez Valdez et al. (2012), Single crystal/DFT
-	170	108	0	Li et al. (1996), Poly-crystal/US
535.8(0.2)	170(2)	115(2)	0	Zha et al. (1997), Single crystal/BS
-	169.7(1.9)-170.7(2)	113.9(0.7)-114.1(0.8)	0	Isaak et al. (2007), Poly-crystal/RUS
541.5	169.5	101.7	0.125	This study, Single crystal/DFT
539.4(4)	170(3)	108(2)	0.08	Sinogeikin et al. (1998), Single crystal/BS
-	170.8(1.2)	108.9(0.4)	0.08	Isaak et al. (2010), Poly-crystal/RUS
-	165.72(6)	105.43(2)	0.09	Mayama et al. (2004), Poly-crystal/RUS
-	172(2)	106(1)	0.12	Li and Liebermann (2000), Poly-crystal/US
-	171.3(3)	108.7(2)	0.13	Liu et al. (2009), Poly-crystal/US
$\gamma-(Mg_{1-x},Fe_x)_2SiO_4$				
V (Å^3)	K (GPa)	G (GPa)	x	Reference
527.6	184.4	120.95	0	This study, Single crystal/DFT
525.3	184	119	0	Weidner et al. (1984), Single crystal/BS
525.3	185(3)	120.4(2)	0	Jackson et al. (2000), Single crystal/BS
-	185(2)	120(1)	0	Li (2003), Poly-crystal/US
-	185(2)	127(1)	0	Higo et al. (2006), Poly-crystal/US
527.7	186.3	115.3	0.125	This study, Single crystal/DFT
526.2(4)	188.3(30)	119.6(20)	0.09	Sinogeikin et al. (2003), Single crystal/BS
-	185.11(0.16)-185.17(0.17)	118.27(0.06)	0.09	Mayama et al. (2005), Poly-crystal/RUS
-	187(2)	116(1)	0.20	Higo et al. (2006), Poly-crystal/US

Table 1: Results on wadsleyite and ringwoodite for volume (V), bulk (K), and shear (G), moduli at ambient pressure and temperature. US: Ultrasonic techniques; BS: Brillouin scattering techniques; RUS: Resonant Ultrasonic techniques.

riched in Ca and Al) at 1400° C, the wadsleyite to ringwoodite phase change produces a strong discontinuity at ∼500–520 km depth, while the exsolution of Ca-perovskite produces a weak discontinuity near 540 km. At 1600° C, the two merge to form a single discontinuity at 540–560 km. In MORB-like compositions, wadsleyite and ringwoodite are effectively absent, but exsolution of Ca-perovskite causes a velocity discontinuity near 560 km. Saikia et al. (2008) concluded that a mechanical mixture (or seismically averaged assemblage) of peridotite and MORB would have two discontinuities: one near 500 km due to the wadsleyite to ringwoodite phase change, and a second near 560 km due to the exsolution of Ca-perovskite from garnet, consistent with a hypothesis of Deuss and Woodhouse (2001).

Of some question here is the association of the MORB-like mantle with the non-MORB component. If MORB is associated with peridotitic mantle, the strength of the 500 km discontinuity would decrease with respect to that of the 520 km proportionally to the percentage of MORB. Since ΔV_S is smaller for the ex-solution of Ca-perovskite from majorite garnet in MORB-like material by a factor of 2 (Saikia et al., 2008), the summed strength of the two seismic discontinuities, at 500 km and 560 km, in a MORB plus peridotite mixture would be smaller than that of the 520 km alone. This is opposite to observations (Deuss and Woodhouse, 2001), and whether this is the result of an upward bias in identifying split arrivals or the result of greater net velocity contrast is not clear. If MORB is associated with MORB-depleted mantle (harzburgite or dunite) the greater wadsleyite fraction in the depleted mantle might compensate and increase in ΔV_S for the 500 km discontinuity. However, the smaller fraction of iron in MORB-depleted mantle

T (K)	1500		1700	
x	0.0	0.125	0.0	0.125
$\Delta\rho$	1.89	1.92	1.91	1.94
ΔK	7.94	8.31	8.13	8.41
ΔG	8.14	10.26	8.42	10.55
ΔV_P	3.07	3.58	3.17	3.67
ΔV_S	3.12	4.17	3.26	4.31
ΔV_Φ	3.03	3.20	3.11	3.23
$\Delta(\rho V_P)$	4.96	4.99	5.08	5.11
$\Delta(\rho V_S)$	5.02	5.04	5.17	5.20

Table 2: Predicted contrasts in % across the $\beta \rightarrow \gamma$-$(Mg_{1-x},Fe_x)_2SiO_4$ transition at 18 GPa.

(Jaques and Green, 1980) should decrease ΔV_S (as shown in Table 2) of the β to γ transition. The extent to which these effects counter-act each other and whether the greater summed strength of the two discontinuities can be explained by this picture, remains an open question.

5. Conclusions

For the first time, we have presented parameter-free first-principles results of high pressure and high temperature aggregate elastic properties and sound velocities of Fe-bearing ringwoodite. We used the QHA and a novel method of calculating elasticity at high temperatures (Wu and Wentzcovitch, 2011). Treatment of strain Grüneisen parameters via isotropic averages reduced greatly the computational cost of the task, which, otherwise, would have been

much more intensive and lengthy. Within the QHA limit, our predictions for elastic and acoustic properties for $x = 0$ were found to be in very good agreement with available experimental data at 300 K and ambient pressure (Li et al., 1996; Zha et al., 1997; Isaak et al., 2007; Li, 2003; Higo et al., 2006; Weidner et al., 1984) and molecular dynamics simulations (Li et al., 2006) at high pressures and temperatures. For $x = 0.125$ our results compared very well with experimental data in the range $x = 0.08 - 0.2$ (Sinogeikin et al., 1998; Li and Liebermann, 2000; Liu et al., 2009; Sinogeikin et al., 2003; Higo et al., 2006). High-temperature and ambient pressure results in ringwoodite also reproduced experimental trends very well (Isaak et al., 2007; Mayama et al., 2004; Isaak et al., 2010; Jackson et al., 2000; Mayama et al., 2005; Sinogeikin et al., 2003) for Fe-free and Fe-bearing samples.

Overall our predictions showed well defined changes in the elastic and acoustic properties of the $\beta-$ and $\gamma-$ phases near conditions of the 520 km seismic discontinuity. We show that pressure tends to decrease contrasts across the $\beta \rightarrow \gamma$ transition while temperature and iron concentration tend to enhance them. The absence of global observations of the 520 km discontinuity could suggest regions of the TZ with less iron and/or smaller olivine content and irregular temperature topography. Other considerations to try to explain the intermittent nature of the discontinuity would involve changes in the pyroxene/garnet/Ca-pv system and the amount of water present in the TZ. These issues will be addressed in future similar studies including other relevant phases.

6. Acknowledgments

Research supported by the NSF/EAR-1019853, and EAR-0810272. Computations were performed using the VLab cyberinfrastructure at the Minnesota Supercomputing Institute.

References

Abramson, E.H., J. M. Brown, L. J. Slutsky, and J. Zaug, 1997. The elastic constants of San Carlos olivine to 17 GPa, Geophys. Res.,102, 12253–12263.

Akaogi, M., E. Ito, and A. Navrotsky, 1989. Olivine-modified spinel-spinel transitions in the system Mg_2SiO_4-Fe_2SiO_4: Calorimetric measurements, thermochemical calculation, and geophysical application, J. Geophys. Res., 94, 15 671–15 685.

Bagley, B., A. M. Courtier, and J. Revenaugh, 2009. Melting in the deep upper mantle oceanward of the Honshu slab, Physics of the Earth and Planetary Interiors, 175 (3-4), 137–144.

Baroni, S., A. Dal Corso, S. de Gironcoli, and P. Gianozzi, 2001. Phonons and related crystal properties from density-functional perturbation theory, Rev. of Mod. Phys., 73(2), 515 LP–562 LP.

Carrier, P., R. M. Wentzcovitch, and J. Tsuchiya, 2007. First principles prediction of crystal structures at high temperatures using the quasiharmonic approximation, Phys. Rev. B 76, 064116.

303 Ceperley, D. M., and B. J. Alder, 1980. Ground state of the electron gas by
304 a stochastic method, Phys. Rev. Lett., 45, pp. 566–569.

305 Chambers, K., A. Deuss, and J. Woodhouse, 2005. Reectivity of the 410-km
306 discontinuity from PP and SS precursors, Journal of Geophysical Research,
307 110 (B2), 1–13

308 Da Silveira, P., C. R. S. da Silva, and R. M. Wentzcovitch, 2008. Meta-
309 data management for distributed first principles calculations in VLab–A
310 collaborative cyberinfrastructure for materials computation, Comp. Phys.
311 Comm., 178, 186.

312 Da Silveira, P., M. Nez Valdez, R. M. Wentzcovitch, M. Pierce, and D. A.
313 Yuen, 2011. VLab: an updated overview of system service and architecture,
314 Proc. of Teragrid 2011 Conference, in press.

315 Deuss, A., and J. Woodhouse 2001. Seismic observations of splitting of the
316 mid-transition zone discontinuity in Earths mantle., Science, 294 (5541),
317 354–7.

318 Giannozzi P. et al., 2009. QUANTUM ESPRESSO: a modular and open-
319 source software project for quantum simulations of materials, J. Phys.:
320 Condens. Matter, 21, 395502. http://www.quantum-espresso.org

321 Higo, Y., T. Inoue, B. Li, T. Irifune, and R. C. Liebermann, 2006. The effect
322 of iron on the elastic properties of ringwoodite at high pressure, Phys.
323 Earth Planet. Inter., 159 pp. 276–285.

324 Hohenberg, P., and W. Kohn, 1964. Inhomogeneous Electron Gas, Phys.
325 Rev., 136, B864–871.

326 Irifune, T., and A.E. Ringwood, 1987. Phase transformations in primitive
327 MORB and pyrolite compositions to 25 GPa and some geophysical impli-
328 cations, In: M. Manghnani and Y. Syono, Editors, High pressure Research
329 in Geophysics, TERRAPUB/AGU, Tokyo/Washington, D.C. (1987), pp.
330 231–242

331 Isaak, D. G., O. L. Anderson, T. Goto, and I. Suzuk,1989. Elasticity of single-
332 crystal forsterite measured to 1700 K, J. Geophys. Res., 94, 5895–5906.

333 Isaak, 1992. D. G. High-Temperature Elasticity of Iron-Bearing Olivines, J.
334 Geophys. Res., 97, 1871–1885, 1992.

335 Isaak, D. G., G. D. Gwanmesia, D. Falde, M. G. Davis, R. S. Triplett, and l.
336 Wang, 2007. The elastic properties of $\beta-Mg_2SiO_4$ from 295 to 660 K and
337 implications on the composition of Earth's upper mantle, Phys. Earth and
338 Plan. Int., 162, 22–37.

339 Isaak, D. G., G. D. Gwanmesia, M. G. Davis, S. C. Stafford, A. M. Stafford,
340 and R. S. Triplett, 2010. The temperature dependence of the elasticity of
341 Fe-bearing wadsleyite, Phys. Earth Planet. Int., 182, 107–112.

342 Jaques, A. L., and Green, D. H., 1980. Anhydrous melting of peridotite at
343 0–15 kb pressure and the genesis of tholeiitic basalts. Contributions to
344 Mineralogy and Petrology, 73, 287–310.

345 Jackson, J. M., S. V. Sinogeikin, and J. D. Bass, 2000. Sound velocities
346 and elastic properties of $\gamma-(Mg_2SiO_4$ to 873 K by Brillouin spectroscopy,
347 Amer. Mineral., 85, 296–303.

Kohn, W., and L. J. Sham (1964), Self-Consistent equations including exchange and correlation effects, Phys. Rev.,140, A1133–1138.

Katsura, T and E. Ito, 1989. The system Mg_2SiO_4-Fe_2SiO_4 at high pressures and temperatures: Precise determination of stabilities of olivine, modified spinel and spinel. J. Geophys. Res., 94, 15 663–15 670.

Lawrence, J. F., P. M. Shearer, 2000. Constraining seismic velocity and density for the mantle transition zone with reflected and transmitted waveforms, Geochem. Geophys. Geosyst., 7, Q10012.

Li, B., G. D. Gwanmesia, and R. C. Liebermann, 1996. Sound velocities of Olivine and Beta Polymorphs of Mg_2SiO_4 at Earth's Transition Zone Pressures, Geophys. Res. Lett., 23, 2259.

Li, B., and R. C. Liebermann, 2000. Sound velocities of wadsleyite $\beta-(Mg_0.88,Fe_0.12)_2SiO_4$ to 10 GPa, American Mineralogist, 85, 292–295.

Li, B., 2003. Compressional and shear velocities of ringwoodite $\gamma-(Mg_2SiO_4$ to 12 GPa, American Mineralogist, 88, 1312–1317.

Li, L., D. J. Weidner, J. Brotholt, D. Alfè, and G. D. Price, 2006. Elasticity of (Mg_2SiO_4 ringwoodite at mantle conditions, Phys. Earth Planet. Int., 157, 181–187.

Li, B., and R. C. Liebermann, 2007. Indoor seismology by probing the Earth's interior by using sound velocity measurements at high pressures and temperatures, Proceedings of the National Academy of Sciences, 9145–9150.

Liu, W., J. Kung, B. Li, N. Nishiyma, and Y. Wang, 2009. Elasticity of $\beta-(Mg_0.87,Fe_0.13)_2SiO_4$ wadsleyite to 12 GPa and 1073 K, Phys. Earth Planet. Int., 174, 98–104.

Mayama, N., I. Suzuki, and T. Saito, 2004. Temperature dependence of elastic moduli of $\beta-(Mg_{1-x},Fe_x)_2SiO_4$, J. Geophys. Res., 31, L04612.

Mayama, N., I. Suzuki, T. Saito, I. Ohno, T. Katsura, and A. Yoneda, 2005. Temperature dependence of elastic moduli of ringwoodite, Phys. Earth Planet. Int., 148, 353–359.

Núñez Valdez, M., K. Umemoto, and R. M. Wentzcovitch, 2010. Fundamentals of elasticity of $(Mg_{1-x},Fe_x)_2SiO_4$-olivine, Geophys. Res. Lett., 37, L14308.

Núñez Valdez, M., P. da Silveira, and R. M. Wentzcovitch, 2011. Influence of Iron on the Elastic Properties of Wadsleyite and Ringwoodite, J. Geophys. Res., 116, B12207.

Núñez Valdez, Z. Wu, Y. G. Yu and R. M. Wentzcovitch, 2012. Thermoelastic Properties of Olivine and Wadsleyite $(Mg_{1-x},Fe_x)_2SiO_4$: Their Relationship to the 410 km Seismic Discontinuity, Geophys. Res. Lett., under review.

Putnis, A., 1992. Introduction to Mineral Sciences, 399 pp., Cambridge University Press, UK

Revenaugh, J., T.H. Jordan, 1991. Mantle layering from ScS reverberations. 2. The Transition zone, J. Geophys. Res., 96, 19,763–19,780.

391 Rigden, S.M., G. D. Gwanmesia, J. D. Fitz Gerald, I. Jackson, and R. C.
392 Liebermann, 1991. Spinel elasticity and seismic structure of the transition
393 zone of the mantle, Nature, 354, 143–145.

394 Rigden, S.M., G. D. Gwanmesia, I. Jackson, and R. C. Liebermann, 1992.
395 Progress in high-pressure dependence of elasticity of Mg_2SiO_4 polymorphs
396 and constraints on the composition of the transition zone of the Earth's
397 mantle. In: Syono, Y., Manghnani, M.H. (Eds.), High-Pressure Research:
398 Application to Earth and Planetary Science. Geophys. Monogr. Ser. 67,
399 Am. Geophys. Union, 167–182

400 Rinwood, A.E., 1975. Composition an petrology of he Earth's mantle, 618
401 pp., McGraw-Hill, New York

402 Saikia, A., D. J. Frost, and D. C. Rubie (2008). Splitting of the 520-kilometer
403 seismic discontinuity and chemical heterogeneity in the mantle, Science,
404 319(5869),1515–1518.

405 Shearer, P. M. (1990). Seismic imaging of upper-mantle structure with new
406 evidence for a 520-km discontinuity, Nature, 344 (6262), 121–126.

407 Sinogeikin, S. V., J. D. Bass, A. Kavner, and R. Jeanloz, 1997. Elasticity of
408 natural majorite and ringwoodite from the Catherwood meteorite, Geo-
409 phys. Res. Lett., 24(24), 3265–3268.

410 Sinogeikin, S. V., T. Katsura, and J. D. Bass, 1998. Sound velocities and
411 elastic properties of Fe-bearing wadsleyite and ringwoodite, J. Geophys.
412 Res., 103(B9), 20,819–20,825.

413 Sinogeikin, S. V., J. D. Bass, and T. Katsura, 2003. Single-crystal elasticity
414 of ringwoodite to high pressures and high temperatures: implications for
415 520 km seismic discontinuity, Phys. Earth Planet. Inter.,136, 41–66.

416 Stackhouse, S., L. Stixrude, B. B. Karki, 2010. Determination of the high-
417 pressure properties of fayalite from first-principles calculations, Earth and
418 Planet. Sc. Lett.289, 449–456.

419 Vanderbilt, D., 1990. Soft self-consistent pseudopotentials in a generalized
420 eigenvalue formalism, Phys. Rev. B,41, R7892.

421 Wallace, D. C., 1972. Thermodynamics of Crystals, John Wiley& Sons, Inc.,
422 USA.

423 Watt, J. P., G. F. Davies, and R. J. O'Connell, 1976. The Elastic Properties
424 of Composite Materials, Rev. of Geoph. and Spac. Phys., 50, 6290–6295.

425 Watt, J. P., 1979. Hashin-Shtrikman bounds on the effective elastic moduli of
426 polycrystals with orthorhombic symmetry, J. Appl. Phys., 50, 6290–6295.

427 Weidner, D. J., H. Sawamoto, S. Sasaki, and M. Kumazawa, 1984. Single-
428 crystal elastic properties of the spinel phase of Mg_2SiO_4, J. Geophys. Res.,
429 89(B9), 7852–7860.

430 Wentzcovitch, R. M., 1991. Invariant molecular dynamics approach to struc-
431 tural phase transitions, Phys. Rev. B, 44, 2358–2361.

432 Wentzcovitch, R. M., J. L. Martins, and G. D. Price, 1993. *Ab initio* molec-
433 ular dynamics with variable cell shape: application to $MgSiO_3$ perovskite,
434 Phys. Rev. Lett., 70, 3947–3950.

435 Wu, Z. and Wentzcovitch R. M., 2011. Quasiharmonic thermal elasticity of
436 crystals: An analytical approach. Phys. Rev. B 83, 184115

437 Y. Yu, Z. Wu, and R. M., Wentzcovitch, 2008. $\alpha \leftrightarrow \beta \leftrightarrow \gamma$ transformations in
438 Mg_2SiO_4 in Earth's transition zone, Earth Planet. Sci. Lett., 273, 115-122.

439 Zha, C.S., T.S. Duffy, H.W. Mao, R.T. Downs, R.J. Hemley and D.J. Weid-
440 ner, 1997), Single-crystal elasticity of β-Mg_2SiO_4 to the pressure of the 410
441 km seismic discontinuity in the earth's mantle, Earth Planet. Sci. Lett.,
442 147, E9–E15